

Germanium core-level shifts at Ge/GeO₂ interfaces through hybrid functionals

Jan Felix Binder, Peter Broqvist,* Hannu-Pekka Komsa, and Alfredo Pasquarello

Chaire de Simulation à l'Echelle Atomique (CSEA), Ecole Polytechnique Fédérale de Lausanne (EPFL), CH-1015 Lausanne, Switzerland

(Received 5 March 2012; published 11 June 2012)

The Ge core-level shift across the Ge/GeO₂ interface is determined within semilocal and hybrid density functional schemes. We first assess the accuracy achieved within these theoretical frameworks by comparing calculated and measured core-level shifts for a set of Ge-based molecules. The comparison with experimental data results in rms deviations of 0.19 and 0.09 eV for core-level shifts calculated with semilocal and hybrid density functionals, respectively. We also compare calculated core-level shifts at the Ge(001)-c(4 × 2) surface with high-resolution x-ray photoemission spectra finding similar agreement. We then turn to the Ge/GeO₂ interface, which we describe with atomistic superlattice models showing alternating layers of Ge and GeO₂. The adopted models include a substoichiometric transition region in which all Ge atoms are fourfold coordinated and all O atoms are twofold coordinated, as inferred for Si/SiO₂ interfaces. Since the calculation of core-level shifts involves charged systems subject to finite-size effects, we use two different methods to ascertain the core-level shift ΔE_{XPS} between the oxidation state Ge⁰ and Ge⁺⁴ across the interface. In the first method, core-hole relaxations are first evaluated in bulk models of the interface components and then complemented by the initial-state shift calculated across the interface, while the second method consists of direct interface calculations corrected through classical electrostatics. Using the more accurate hybrid functional scheme, we obtain a shift ΔE_{XPS} of 2.7 ± 0.1 eV. This value is significantly lower than experimental data, which typically fall around 3.3 eV or higher, but the underestimation is consistent with that found for the valence band offset of the same model. This leads to the conclusion that the adopted model structures yield an incorrect description of the interface dipole and emphasizes that Ge/GeO₂ interfaces possess different structural properties than their silicon counterparts.

DOI: [10.1103/PhysRevB.85.245305](https://doi.org/10.1103/PhysRevB.85.245305)

PACS number(s): 79.60.Jv, 73.20.-r, 68.35.bg, 71.15.Mb

I. INTRODUCTION

In order to meet future demands in terms of speed and power consumption for microelectronic devices, alternatives to the silicon-based technology are currently being investigated. In this context, germanium has been shown to display several advantages over silicon for use in field-effect transistors.¹ For instance, the mobilities of both holes and electrons are significantly higher and the lower band gap makes it possible to operate devices at lower voltages.¹ Another advantage is that germanium requires lower temperatures for dopant activation which might allow for an easier integration with a high- κ dielectric material like HfO₂.¹ However, germanium-oxide interfaces generally show considerably higher defect densities than their silicon counterparts.² To make progress, it is important to achieve a detailed understanding of the electronic and structural properties of Ge/GeO₂ interfaces.

X-ray photoemission spectroscopy (XPS) is a standard analytical tool for the characterization of semiconductor/oxide interfaces. Core electrons are emitted and their binding energy is inferred from their kinetic energy. At Ge/GeO₂ interfaces, this technique is sensitive to the local structure around Ge atoms and to the electrostatic discontinuity at the interface. For Ge/GeO₂ interfaces grown by thermal oxidation, a shift of $\Delta E_{\text{XPS}} = 3.3 \pm 0.1$ eV is generally measured for the Ge 3d core level between nonoxidized Ge in the substrate and fully oxidized Ge in GeO₂.³⁻⁸ In experiments in which the interfaces are grown with oxidizing agents such as O₃ and atomic O, much larger values (3.7–3.8 eV) have been reported.^{9,10} The spread in the experimental values likely results from the different growth conditions.

The measured XPS shifts can be used to derive valence band offsets (VBOs) through the application of Kraut's method.^{11,12}

For the interfaces grown with reactive O species, this method yielded VBOs around 4.5 eV.^{9,10} Valence band offsets can alternatively be obtained directly from photoemission spectra in which the onsets of the valence band edges of both Ge and GeO₂ appear. This direct procedure has been found to yield a VBO of 4.0 eV for Ge/GeO₂ interfaces obtained by thermal oxidation,⁵ while a larger VBO value is confirmed for structures grown by O₃ oxidation (4.3 eV).⁹ Overall, on the basis of the available experimental data,^{5,9} it appears that the shift ΔE_{XPS} and the VBO vary consistently, supporting that the interfaces achieved with different growth conditions differ in their band alignment.

Several studies have addressed the electronic properties at the Ge/GeO₂ interface. This interface is generally modeled in the same way as Si/SiO₂ interfaces,¹³⁻¹⁸ namely through the consideration of a substoichiometric transition region in which all Ge atoms are fourfold coordinated and all O atoms are twofold coordinated.^{19,20} For an interface of this type, Pourtois *et al.* performed density-functional calculations within the local density approximation finding a Ge 3d shift across the interface of $\Delta E_{\text{XPS}} = 3.2$ eV,¹⁴ in excellent agreement with measurements at thermally oxidized structures (3.3 ± 0.1 eV).³⁻⁸

The theoretical determination of VBOs suffers from the severe band-gap underestimations inherent to standard semilocal density functionals.¹⁵ To overcome these limitations, one can turn to hybrid density functionals, which have been shown to yield accurate band alignments for a series of semiconductor-oxide interfaces.²¹ However, such an approach applied to Ge/GeO₂ interfaces yielded VBOs of about 3.4 eV,^{15,18} noticeably lower than the experimental value expected for thermally oxidized interfaces (4.0 eV).⁵ The theoretical situation is further complicated by a recent study at the hybrid functional

level which yields a VBO of 4.3 eV for similarly constructed models.¹⁷ Hence, severe inconsistencies subsist among the various theoretical descriptions.

It has recently been suggested that substoichiometric GeO_x has fundamentally different bonding characteristics than its Si analog, showing the occurrence of valence alternation pairs.²² These consist of negatively charged Ge dangling bonds and positively charged threefold coordinated O atoms. It has further been shown that such pairs may significantly contribute to the interface dipole and thus affect the band alignment.¹⁸ Hence, the band alignment acts as a fingerprint of the underlying interface structure. This calls for theoretical efforts aiming at an accurate quantitative description, which consistently accounts for both the XPS shift and the VBO.

In this work, we determine in an accurate way the Ge $3d$ core-level shift across the Ge/GeO₂ interface using a plane-wave pseudopotential scheme at the hybrid density functional level of theory. The ultimate aim of this paper is to clarify the relation between measured core-level shifts and the underlying structural properties of the Ge/GeO₂ interface. For this purpose, it is important to achieve high quantitative accuracy in the calculated Ge core-level shifts. We begin our study by assessing the overall accuracy associated to our determination of Ge core-level shifts in molecules by comparison with experimental data. This study on molecules gives two main results: (i) It shows that calculated Ge core-level shifts generally differ from experiment by less than 0.1 eV with hybrid functionals achieving a small quantitative improvement with respect to semilocal functionals; (ii) it allows us to verify the validity of our pseudopotential approach when moving from an all-electron description to a pseudopotential one. As a side result, we also find that differences between Ge $3d$ and $2p$ shifts are negligible. The achieved level of accuracy enables a quantitative comparison with experiment for the Ge core-level shift across the Ge/GeO₂ interface. To model the interface, we use atomistic structures containing only fourfold-coordinated Ge atoms and twofold-coordinated O atoms. These models enable us to achieve a comprehensive description of electronic properties at Ge/GeO₂ interfaces, since calculated VBOs for these same models are already available.^{15,18} Since the core-level shift determination involves charged supercell calculations, the convergence due to finite-size effects needs to be carefully ensured. Thus, the core-level shift calculations at the interface are performed through the use of two different methods. In the first method, we adopt a two-step procedure in which the core levels are separately determined in bulk models of the two interface components and then aligned through a local reference potential determined at the interface. The second method is based on core-level shift calculations performed directly at the interface. To cope with the spurious effect of periodic boundary conditions, we correct our results for finite-size effects using classical electrostatics. The overall agreement between the two schemes allows us to assess whether the adopted interface model structures are consistent with experimental data.

This paper is organized as follows. In Sec. II, we describe the electronic-structure methods for the determination of core-level shifts used in this work. In Sec. III, Ge core-level shifts are determined at various levels of theory for atoms, molecules, and Ge surfaces, and compared to experimental

data when available. We turn to the core-level shift at the Ge/GeO₂ interface in Sec. IV, where two calculation methods are confronted. The paper concludes with Sec. V, where the implications of our results are discussed.

II. METHODS

Total energies are obtained from electronic structure calculations based on density functional theory. We used two different density functionals. The first is the semilocal density functional proposed by Perdew, Burke, and Ernzerhof (PBE).²³ The second is a hybrid functional which is obtained from the semilocal PBE functional by replacing a fraction α of the exchange functional with Fock exchange:

$$E_x = \alpha E_x^{\text{Fock}} + (1 - \alpha) E_x^{\text{PBE}}. \quad (1)$$

This hybrid functional is referred to as PBEh(α) and corresponds to the PBE0 functional when $\alpha = 0.25$.²⁴

As we treat systems of increasing complexity, we adapt the applied electronic-structure calculation scheme. In this work we use three different schemes. The first scheme assumes spherical symmetry and is here only used for all-electron calculations at the PBE level for the Ge atom and its excited states. The radial Kohn-Sham equations are integrated numerically with different spin channels treated separately. Relativistic effects are included in the scalar approximation.²⁵ These calculations are performed with the ATOMIC code²⁶ provided in the QUANTUM-ESPRESSO package.²⁷

In order to extend the all-electron calculations to molecular systems and to hybrid functionals, we use an electronic-structure scheme based on local basis sets, as implemented in the ADF code.²⁸ The ADF code employs Slater-type orbitals as basis functions. The basis functions are extended to include diffuse functions to treat atomic excitations involving weakly bonded $4d$ states when appropriate. Relativistic effects are treated in the zeroth-order regular approximation.²⁹ The electronic-structure calculations on molecules are performed at the all-electron level with triple- ζ (TZ2P) basis sets. In the structural optimizations, the convergence criteria are set at 1 mHa for the total energy and at 1 mHa/Å for the remaining maximal force. The molecular structures are relaxed within this structural relaxation scheme.

To address the Ge/GeO₂ interface system, we use a plane-wave density functional approach in which core-valence interactions are described by normconserving pseudopotentials.³⁰ For Ge, we include a nonlinear core correction to account for the overlap between core and valence electron densities. The pseudopotentials are generated at the PBE level of theory, and used in all calculations. While this practice is conceptually not satisfactory for hybrid functionals, it is demonstrated below through comparison with all-electron schemes that it does not lead to any sizable error in the core-level calculations. The valence electron wave functions are expanded in plane-wave basis sets defined by an energy cutoff of 70 Ry. The structural optimizations are performed at the PBE level with convergence criteria of 0.1 mRy for the total energy and 1 mRy/bohr for the maximal residual force. The singularity of the exchange potential is treated with an auxiliary function.^{31,32} We used the PWSCF code provided in the QUANTUM-ESPRESSO package.²⁷

We model the core-electron binding energy E_b measured in XPS experiments as the energy required to excite the electron from its core level to the vacuum level:

$$E_b = E^+ + V_{\text{vac}} - E^0, \quad (2)$$

where E^+ is the final-state energy of the system in the presence of a core hole, V_{vac} the reference vacuum potential for the extracted electron, and E^0 the energy of the initial state. We assume the vertical approximation which implies that the atomic structure is not modified in the final state and that polarization effects are described by the high-frequency dielectric constant. In our all-electron schemes, the final state energy E^+ is obtained through a calculation in which the occupation of the core state is constrained. This corresponds to the evaluation of core-level binding energies through the Δ SCF method.³³

More specifically, we focus in this work on core-level shifts with respect to an adopted reference:

$$\Delta E_b = (E^+ - E^0) - (E_{\text{ref}}^+ - E_{\text{ref}}^0). \quad (3)$$

Such core-level shifts then become also accessible in the pseudopotential scheme. For this purpose, a special pseudopotential is generated for describing the valence electrons in the presence of a core hole.³⁴ With respect to all-electron schemes, the pseudopotential approach does not account for the relaxation of core electrons. This approximation is generally very good, as demonstrated for the analogous Si/SiO₂ interface.^{35–37}

In the pseudopotential calculations, the presence of the core hole requires a uniform background charge to achieve charge neutrality in the periodically repeated simulation cell. Spurious interaction effects due to the periodic boundary conditions might affect the calculated results and need to be accounted for. For the molecular systems, we calculated core-level shifts using cubic simulation cells with sides increasing from 20 to 30 bohr. The desired shifts could then be obtained through extrapolation to infinite cell size.^{37,38} For the interface systems, the effect due to the dielectric discontinuity is less trivially determined. Special attention to the ensuing corrections will be given in Sec. IV D.

III. ACCURACY OF ADOPTED APPROACH

A. Atom

The atom is the most simple case for which core-level shifts can be calculated and is therefore a suitable test case to perform a comparison between different theoretical schemes. In particular, we are interested in validating the local basis sets used in the all-electron scheme. To this end, we here first validate the basis sets through comparisons with results obtained through numerical integration, which are not subject to basis set errors. Then, we compare core-level shifts calculated at the PBE and PBE0 levels of theory. The section concludes with a comparison between Ge $3d$ and Ge $2p$ core-level shifts.

To validate the local basis sets, we focus on Ge atoms imposing spherical symmetry. The core-level binding energies are given with respect to the ground state Ge atom in the electronic configuration $[\text{Ar}]3d^{10}4s^24p^2$. In Table I, Ge $3d$ core-level shifts obtained through numerical integration are compared with those obtained with three different local basis sets for various electronic configurations of the outer valence shells. We consider the triple- ζ basis set with two

TABLE I. Calculated $3d$ core-level shifts for the Ge atom in various excited electronic configurations of the outer valence shells with respect to the ground-state configuration $[\text{Ar}]3d^{10}4s^24p^2$. The exact core-level shifts are obtained through numerical integration of the Kohn-Sham equations (ATOMIC code, Ref. 27) and are compared to those obtained with three different local basis sets (ADF code, Ref. 28). The calculations are performed at the PBE level of theory. Energies are in eV.

Configuration	Exact	TZ2P	QZ4P	ETQZ3P-3diff
s^1p^3	1.666	1.671	1.668	1.671
$s^2p^1d^1$	4.689	1.252	4.229	4.672
$s^1p^2d^1$	6.113	3.032	5.757	6.100
s^2p^1	10.230	10.239	10.226	10.223
s^1p^2	11.862	11.869	11.859	11.868
$s^1p^1d^1$	15.568	13.932	15.601	15.553

polarization functions (TZ2P), the quadruple- ζ basis set with four polarization functions (QZ4P), and the even-tempered basis set augmented with three polarization functions and three diffuse functions (ETQZ3P-3diff). The calculations are performed at the PBE level of theory.

As seen in Table I, the core-level shifts spread out over a range of more than 15 eV. For the s^1p^3 , s^2p^1 , and s^1p^2 configurations, one notices that the results obtained with the TZ2P and QZ4P basis sets are both very accurate. For describing the excitations to states involving the weakly bound $4d$ level, even the large standard basis set (QZ4P) is not sufficient and a good agreement is only achieved through the use of the ETQZ3P-3diff basis set which includes diffuse functions.

Next, we compare in Table II atomic core-level shifts calculated with the PBE functional with those obtained with the hybrid PBE0 functional. In this comparison, we use the ETQZ3P-3diff basis set to account for the weakly bonded $4d$ levels. We note that the differences for the more localized configurations (s^1p^3 , s^2p^1 , and s^1p^2) never exceed 0.15 eV. This result is in good agreement with the general behavior of charge transition levels of atomically localized defect states.^{39,40} More generally, calculations with the PBEh(α) functional show that the core-level shift dependence on α is linear, in agreement with previous calculations for both localized and extended states.^{21,41} The rate of change is specific to the considered electronic configuration.

The Ge $3d$ level is only slightly deeper than the valence electrons ($E_b \sim 30$ eV), while the Ge $2p$ level is much deeper

TABLE II. Comparison between $3d$ core-level shifts for the Ge atom as calculated with the semilocal PBE and hybrid PBE0 functionals. The ADF code is used with the ETQZ3P-3diff basis set. The last column corresponds to the difference between the PBE0 and PBE shifts. Energies are in eV.

Configuration	PBE	PBE0	Diff.
s^1p^3	1.671	1.814	0.143
$s^2p^1d^1$	4.674	4.959	0.285
$s^1p^2d^1$	6.102	6.543	0.441
s^2p^1	10.224	10.115	0.109
s^1p^2	11.869	11.938	0.069
$s^1p^1d^1$	15.553	15.791	0.238

TABLE III. Comparison between Ge $2p$ and Ge $3d$ core-level shifts calculated with the hybrid PBE0 functional. The ADF code is used with the ETQZ3P-3diff basis set. The difference between Ge $2p$ and Ge $3d$ core-level shifts is given in the last column. Energies are in eV.

Configuration	Ge $3d$	Ge $2p$	Diff.
$s^1 p^3$	1.814	1.831	0.017
$s^2 p^1 d^1$	4.959	4.907	-0.052
$s^1 p^2 d^1$	6.543	6.529	-0.014
$s^2 p^1$	10.115	10.314	0.199
$s^1 p^2$	11.938	12.150	0.212
$s^1 p^1 d^1$	15.791	16.099	0.308

($E_b \sim 1218$ eV).⁵ It is therefore of interest to compare $2p$ and $3d$ core-level shifts as both are experimentally accessible. In Table III, Ge $2p$ core-level shifts calculated with PBE0 functionals are compared with the respective Ge $3d$ shifts. Overall, Ge $3d$ and Ge $2p$ are remarkably similar for shifts up to ~ 6.5 eV and show deviations of at most 0.3 eV for larger shifts.

B. Molecules

The primary aim of this section is to assess the accuracy of Ge core-level shifts calculated within all-electron hybrid density functional schemes. We thus consider a set of molecules for which experimental data are available.⁴² In particular, we determine the optimal value of the fraction α of nonlocal exchange to be used in the hybrid functional PBEh(α). We then switch to the pseudopotential scheme and quantify to what extent this approximation deteriorates the accuracy achieved with the all-electron scheme.

1. Structural properties

The relaxed structures of a set of Ge-based molecules are determined with the PBEh(α) hybrid functional for various values of α . We here use the all-electron ADF code with the TZ2P basis set, which is expected to give converged core-level shifts in the absence of diffuse d electrons (cf. Table I). Table IV shows relaxed structural parameters for the two extreme values $\alpha = 0$ (PBE) and $\alpha = 1$. Overall, the effect of α is small with bond lengths and bond angles differing by less than 0.1 Å and 2° , respectively.

To illustrate these calculations in more detail, we focus on the $\text{Ge}(\text{CH}_3)_4$, GeH_4 , and GeF_4 molecules and give in Fig. 1 the evolution of three specific bond lengths with α . The bond lengths vary in an approximately linear way with α . For $\alpha = 0$ (PBE), they are slightly larger than their experimental counterparts, while the opposite behavior is found for $\alpha = 1$. The best agreement with experiment is found for $\alpha \cong 0.5$. As will be seen below, the structural variations observed here can be considered to be marginal since they do not have a significant impact on the calculated core-level shifts.

2. Ge $3d$ core-level shifts

Ge $3d$ core-level shifts are calculated within an all-electron scheme for the set of molecules in Table IV. For each molecule, the calculations are performed with the PBEh(α) functional for three to five different values of α (ADF code with TZ2P basis set). The molecular structures used in the binding energy

TABLE IV. Bond lengths and bond angles for a set of Ge-based molecules obtained with PBEh(α) functionals for $\alpha = 0$ (PBE) and $\alpha = 1$. The all-electron ADF code is used with the TZ2P basis set.

Molecule	Parameter	$\alpha = 0$	$\alpha = 1$
$\text{Ge}(\text{CH}_3)_4$	$d(\text{Ge-C})$	1.979 Å	1.931 Å
$(\text{CH}_3)_3\text{GeH}$	$d(\text{Ge-H})$	1.551 Å	1.517 Å
	$d(\text{Ge-C})$	1.975 Å	1.926 Å
	$\angle \text{H-Ge-C}$	108.3°	108.0°
$(\text{CH}_3)_2\text{GeH}_2$	$d(\text{Ge-H})$	1.546 Å	1.513 Å
	$d(\text{Ge-C})$	1.970 Å	1.922 Å
	$\angle \text{C-Ge-C}$	111.7°	112.7°
	$\angle \text{H-Ge-C}$	109.4°	109.2°
	$\angle \text{H-Ge-H}$	107.4°	107.3°
$(\text{CH}_3)\text{GeH}_3$	$d(\text{Ge-H})$	1.541 Å	1.508 Å
	$d(\text{Ge-C})$	1.964 Å	1.918 Å
	$\angle \text{H-Ge-C}$	110.6°	110.6°
	$\angle \text{H-Ge-H}$	108.4°	108.3°
GeH_4	$d(\text{Ge-H})$	1.533 Å	1.503 Å
GeH_3Br	$d(\text{Ge-H})$	1.534 Å	1.499 Å
	$d(\text{Ge-Br})$	2.332 Å	2.258 Å
	$\angle \text{H-Ge-H}$	111.4°	111.5°
	$\angle \text{H-Ge-Br}$	107.4°	107.3°
GeH_3Cl	$d(\text{Ge-H})$	1.533 Å	1.499 Å
	$d(\text{Ge-Cl})$	2.175 Å	2.108 Å
	$\angle \text{H-Ge-H}$	111.7°	111.7°
	$\angle \text{H-Ge-Cl}$	107.1°	107.2°
$(\text{CH}_3)\text{GeHF}_2$	$d(\text{Ge-H})$	1.534 Å	1.495 Å
	$d(\text{Ge-C})$	1.939 Å	1.888 Å
	$\angle \text{H-Ge-C}$	121.5°	119.7°
	$\angle \text{F-Ge-C}$	108.5°	109.0°
$(\text{CH}_3)\text{GeCl}_3$	$d(\text{Ge-Cl})$	2.162	2.083 Å
	$d(\text{Ge-C})$	1.949	1.889 Å
	$\angle \text{H-C-Ge}$	108.5°	109.2°
	$\angle \text{Cl-Ge-C}$	111.2°	111.7°
GeBr_4	$d(\text{Ge-Br})$	2.316 Å	2.226 Å
GeCl_4	$d(\text{Ge-Cl})$	2.143 Å	2.065 Å
GeF_4	$d(\text{Ge-F})$	1.713 Å	1.639 Å

calculations are optimized at the corresponding level of theory. The calculated binding energies are found to vary linearly with α .

Since we focus in this work on the accuracy of core-level shifts, we take one molecule as reference and compare calculated and experimental values for the resulting core-level shifts. In this way, systematic errors inherent to the absolute binding energies, such as those resulting from the relativistic approximation used, do not affect the comparison with experiment. Taking the GeH_4 molecule as reference, we calculate the rms deviation $\sigma_{\text{GeH}_4}(\alpha)$ with respect to experimental data⁴² for the set of calculated binding energies obtained with the functional PBEh(α):

$$\sigma_{\text{GeH}_4}(\alpha) = \sqrt{\frac{1}{N-1} \sum_i^N [\delta E_b^i(\alpha) - \delta E_b^i(\text{expt.})]^2}, \quad (4)$$

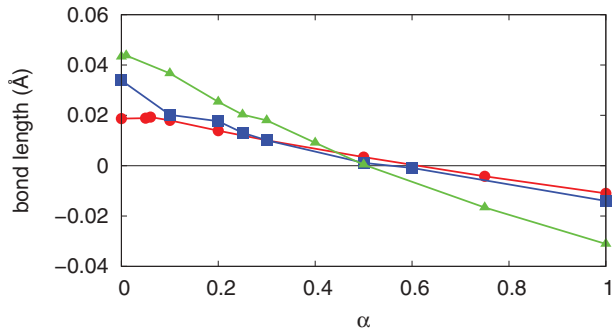


FIG. 1. (Color online) Dependence of the Ge-C, Ge-H, and Ge-F bond lengths on the fraction α of nonlocal exchange for the molecules Ge(CH₃)₄ (squares, blue), GeH₄ (disks, red), and GeF₄ (triangles, green), respectively. The ADF code is used with the TZ2P basis set. The bond lengths are given as deviations with respect to experimental values: $d_{\text{Ge-C}} = 1.945 \text{ \AA}$ (Ref. 43), $d_{\text{Ge-H}} = 1.514 \text{ \AA}$ (Ref. 44), and $d_{\text{Ge-F}} = 1.67 \text{ \AA}$ (Ref. 45).

where $\delta E_b^i(\alpha)$ and $\delta E_b^i(\text{expt.})$ correspond to theoretical and experimental core-level shifts referred to GeH₄ and where the sum is over the molecules in the considered set.

In Table V, we show the comparison with experiment for binding energies calculated with the semilocal PBE functional ($\alpha = 0$) and with the hybrid PBE0 functional ($\alpha = 0.25$), when the GeH₄ molecule is taken as reference. The accuracy of calculated Ge 3*d* core-level shifts can be estimated through σ_{GeH_4} , and results in 0.26 eV for PBE and in 0.08 eV for PBE0. The relative maximal deviations observed are 0.54 and 0.18 eV. These results indicate that core-level shifts obtained

TABLE V. Comparison between calculated and measured Ge 3*d* core-level shifts for a set of Ge-based molecules. We obtain PBE and PBE0 core levels using molecular structures optimized at the corresponding level of theory (ADF code with TZ2P basis set). The calculated and experimental core levels are referred to that of the GeH₄ molecule. We give the rms deviation σ_{GeH_4} obtained for this choice of reference. We also give $\langle\sigma\rangle$ corresponding to the average of all the rms deviations obtained when varying the reference among the molecules in the set. The experimental values are taken from Ref. 42. Energies are in eV.

Molecule	PBE	PBE0	Expt.
Ge(CH ₃) ₄	-1.43	-1.37	-1.27
(CH ₃) ₃ GeH	-1.17	-1.11	-1.05
(CH ₃) ₂ GeH ₂	-0.84	-0.79	-0.72
(CH ₃)GeH ₃	-0.52	-0.45	-0.42
GeH ₄	0	0	0
GeH ₃ Br	0.56	0.66	0.75
GeH ₃ Cl	0.71	0.83	0.87
(CH ₃)GeHF ₂	1.47	1.67	1.62
(CH ₃)GeCl ₃	1.43	1.67	1.71
GeBr ₄	1.70	2.01	2.05
GeCl ₄	2.34	2.63	2.70
GeF ₄	4.11	4.47	4.65
rms deviations			
σ_{GeH_4}	0.26	0.08	–
$\langle\sigma\rangle$	0.19	0.09	–

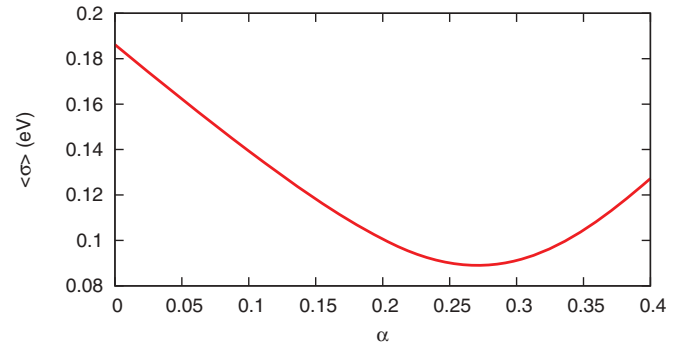


FIG. 2. (Color online) Average deviation $\langle\sigma\rangle$ of relative Ge 3*d* core-level shifts with respect to experimental results as a function of the fraction α of nonlocal exchange used in the PBEh(α) functional. The smallest rms deviation ($\langle\sigma\rangle = 0.09 \text{ eV}$) is achieved for $\alpha = 0.27$.

with the PBE functional are already accurate and that a further improvement can be achieved with the PBE0 functional. The good agreement between PBE and PBE0 shifts is analogously found for ionization potentials in molecules⁴⁶ and defect levels³⁹ in solids, and stems from the localized nature of the core-level state.^{40,47}

While the PBE0 hybrid functional is recommended for a large class of systems, it is admitted that the optimal α might be material or even property dependent.²⁴ Therefore, we investigate how the rms deviation between theoretical and experimental core-level shifts depends on the fraction α of nonlocal exchange. To overcome the arbitrariness of choosing one molecule as reference, we calculate rms deviations taking each molecule as reference in turn and consider the deviation $\langle\sigma\rangle$ resulting from the average of all rms deviations obtained in this way. For each value of α , we first derive theoretical values through the linear interpolation of our results obtained for a limited set of α values. The $\langle\sigma\rangle$ resulting from this procedure are displayed as a function of α in Fig. 2. The minimal value of $\langle\sigma\rangle = 0.09$ is obtained for $\alpha = 0.27$, noticeably improving with respect to $\langle\sigma\rangle = 0.19$ for PBE ($\alpha = 0$). The smallest achieved value of $\langle\sigma\rangle$ does not differ significantly from the one at $\alpha = 0.25$. In the following hybrid functional calculations, we will thus stick to the common PBE0 functional, which corresponds to the latter value of α .

3. Ge 2*p* vs Ge 3*d* core-level shifts

In calculations performed on various excited configurations of the Ge atom, Ge 2*p* and Ge 3*d* core-level shifts are found to be very similar (cf. Sec. III A). To confirm this trend in more general terms, we here compare Ge 2*p* and Ge 3*d* shifts for the considered set of Ge-based molecules. The core-level shift calculations are performed with the PBE0 functional within an all-electron scheme (ADF code with TZ2P basis set). We use atomic coordinates obtained at the same level of theory. The calculated Ge 2*p* and Ge 3*d* core-level shifts are given in Table VI. For the considered set of molecules, the shift ranges over an interval of almost 6 eV, but the difference between the two core-level shifts remains always smaller than 0.1 eV. The similarity of Ge 2*p* and Ge 3*d* core-level shifts is supported by experimental observations.^{4,48} Thus, we only consider Ge 3*d* core-level shifts in the following.

TABLE VI. Comparison between calculated Ge $3d$ and Ge $2p$ core-level shifts in Ge-based molecules. The shifts are determined with the PBE0 hybrid functional in an all-electron scheme (ADF code with TZ2P basis set). The atomic structures used are obtained at the same level of theory. The core levels are referred to respective levels of the GeH₄ molecule. The last column gives the difference between Ge $2p$ and Ge $3d$ shifts. Energies are in eV.

Molecule	$2p$	$3d$	Diff.
Ge(CH ₃) ₄	-1.411	-1.392	-0.019
(CH ₃) ₃ GeH	-1.137	-1.122	-0.015
(CH ₃) ₂ GeH ₂	-0.816	-0.795	-0.021
(CH ₃)GeH ₃	-0.441	-0.454	0.013
GeH ₃ Br	0.726	0.655	0.071
GeH ₃ Cl	0.880	0.892	-0.012
CH ₃ GeHF ₂	1.663	1.660	0.003
CH ₃ GeCl ₃	1.720	1.665	0.055
GeBr ₄	2.084	1.999	0.085
GeCl ₄	2.632	2.595	0.037
GeF ₄	4.386	4.451	-0.065

4. Accuracy of present pseudopotential implementation

In order to address interface models, the pseudopotential scheme is more practical not only because of the lower numerical cost involved but also because of the suitable periodic boundary conditions. However, structural relaxations at the hybrid functional level remain numerically expensive, and it thus appears convenient to use model structures optimized at the semilocal PBE level. In this section, we use the set of Ge-based molecules to quantify the loss of accuracy due to these simplifications.

We first examine the validity of the pseudopotential approximation, in which the relaxation of core electrons upon electron excitation is neglected. For this purpose, we adopt a given atomic configuration of the molecules (corresponding to the geometries obtained at the PBE level) and perform core-level shift calculations at the PBE0 level. By comparing the first two columns in Table VII, one sees that core-level shifts obtained with the pseudopotential scheme are very accurate with deviations with respect to all-electron results lower than 0.06 eV. The comparison with all-electron results is a critical step of the validation process which ensures that the pseudopotential scheme gives quantitatively reliable shifts.⁴⁹

The comparison is then extended to all-electron calculations performed on molecular structures consistently optimized at the hybrid functional level (Table VII). Overall deviations remain below 0.05 eV, indicating that the combined use of the PBE structures and the pseudopotential scheme does not deteriorate the overall accuracy in a significant manner. In particular, we note that the comparison between pseudopotential and all-electron core-level shifts calculated at the PBE0 level does not suffer significantly from the fact that the pseudopotentials are generated at the PBE level of theory, in agreement with previous findings for ionization potentials.³¹

In the last part of this subsection, we use the flexibility of the pseudopotential code to provide deeper insight into the underlying reasons for the overall better performance of PBE0 with respect to PBE. As seen above, the differences between

TABLE VII. Comparison between pseudopotential (PP) and all-electron (AE) Ge $3d$ core-level shifts for various Ge-based molecules calculated at the PBE0 level. The pseudopotential results correspond to structures optimized at the PBE level (\mathbf{R}_{PBE}). The all-electron results (ADF code with TZ2P basis set) are obtained for the same geometries (\mathbf{R}_{PBE}) and for structures consistently optimized at the PBE0 level (\mathbf{R}_{PBE0}). The respective differences between the AE and PP calculations are given by Δ_1 and Δ_2 . The core levels are referred to that of the GeH₄ molecule. Energies are in eV.

Molecule	PP \mathbf{R}_{PBE}	AE \mathbf{R}_{PBE}	Δ_1	AE \mathbf{R}_{PBE0}	Δ_2
Ge(CH ₃) ₄	-1.375	-1.343	0.032	-1.378	-0.002
(CH ₃) ₃ GeH	-1.120	-1.119	0.001	-1.114	0.005
(CH ₃) ₂ GeH ₂	-0.805	-0.792	0.013	-0.792	0.013
(CH ₃)GeH ₃	-0.442	-0.462	-0.020	-0.451	-0.009
GeH ₃ Br	0.700	0.690	-0.010	0.657	-0.043
GeH ₃ Cl	0.863	0.852	-0.011	0.824	-0.039
(CH ₃)GeHF ₂	1.710	1.709	-0.001	1.664	-0.046
(CH ₃)GeCl ₃	1.689	1.714	0.025	1.668	-0.021
GeBr ₄	2.007	2.065	0.058	2.005	-0.002
GeCl ₄	2.630	2.681	0.051	2.625	-0.004
GeF ₄	4.505	4.561	0.056	4.465	-0.040

PBE and PBE0 optimized structures do not affect the core-level shifts in an appreciable way (Table VII). Therefore the effect should be searched in the electronic-structure description. In Table VIII, we compare core-level shifts obtained through a full PBE0 electronic minimization with those obtained through a first-order perturbational scheme based on PBE wave functions. The comparison shows that the differences between the PBE and PBE0 wave functions lead to negligible differences in the core-level shifts. This suggests that the better agreement recorded for the PBE0 core-level shifts should be assigned to the improved energy differences achieved with the PBE0 functional, possibly due to the reduced self-interaction, rather than to an improved description of the wave functions.

TABLE VIII. Comparison between Ge $3d$ core-level shifts obtained self-consistently at the PBE0 level (Ψ_{PBE0}) with those obtained via a perturbational scheme based on PBE wave functions (Ψ_{PBE}), for various Ge-based molecules. The difference between the two shifts is given in the last column. In both calculations, we use the same molecular geometries corresponding to those obtained at the PBE level. The core levels are referred to that of the GeH₄ molecule. Energies are in eV.

Molecule	Ψ_{PBE0}	Ψ_{PBE}	Diff.
Ge(CH ₃) ₄	-1.375	-1.378	-0.002
(CH ₃) ₃ GeH	-1.120	-1.121	-0.002
(CH ₃) ₂ GeH ₂	-0.805	-0.806	-0.001
(CH ₃)GeH ₃	-0.442	-0.442	-0.001
GeH ₃ Br	0.700	0.699	-0.001
GeH ₃ Cl	0.863	0.861	-0.002
(CH ₃)GeHF ₂	1.710	1.702	-0.008
(CH ₃)GeCl ₃	1.689	1.684	-0.005
GeBr ₄	2.007	2.005	-0.002
GeCl ₄	2.630	2.624	-0.005
GeF ₄	4.505	4.490	-0.015

C. Ge(001)- $c(4 \times 2)$ surface

In this section, we continue with the validation of our theoretical approach by calculating Ge $3d$ core-level shifts at the Ge(001) surface. This surface is known to reconstruct through the formation of rows of buckled dimers and has been characterized in detail by high resolution XPS.^{50–53} Given the fact that the surface core-level shifts are at most 0.5 eV, the calculations in this section are only performed at the PBE level. Indeed, for such small shifts the estimated improvement achieved through the use of a hybrid functional would not exceed the overall expected accuracy.

We thus generate a model for the Ge(001) surface showing the $c(4 \times 2)$ dimer reconstruction. In the primitive surface cell, we use 12 Ge layers and 11 Å of vacuum separating the slabs in the z direction normal to the surface. Dangling bonds on the bottom of the slab are terminated with hydrogen atoms to simulate bulk Ge. The four bottom-most Ge layers are kept fixed in bulk positions. For the geometry optimization, we use a $4 \times 4 \times 1$ Monkhorst pack mesh, which is taken to be off-center to avoid the vanishing band gap of Ge at the Γ point. With these settings, the use of the next available denser grid of \mathbf{k} points results in a total-energy change of less than 0.1 meV per atom. The structural relaxation gives a dimer bond of 2.58 Å and a dimer tilt angle of 20.1°, in excellent agreement with previous DFT calculations.⁵⁰ The relaxed structure is illustrated in Fig. 3.

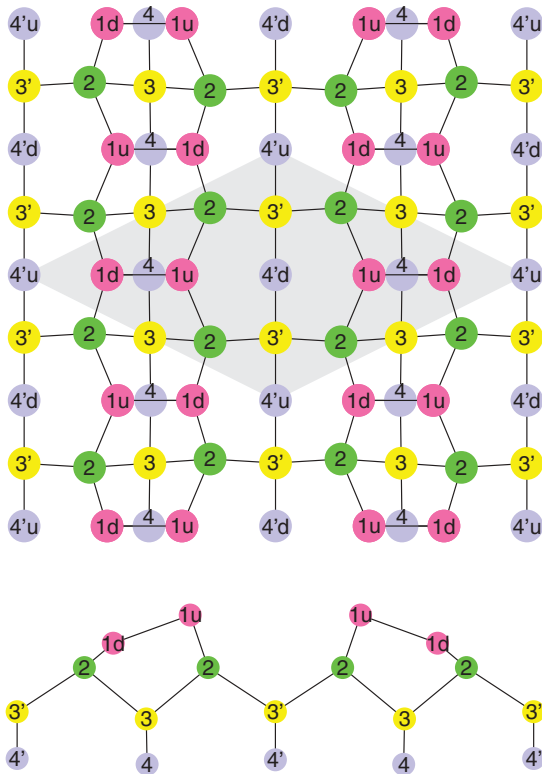


FIG. 3. (Color online) Top view (top panel) and side view (bottom panel) of the Ge(001) surface with the $c(4 \times 2)$ surface reconstruction. The numbers indicate the layers after a common labeling convention (Refs. 35 and 50). Atoms in the same layer share the same level of gray (color). The shaded area shows the primitive surface unit cell.

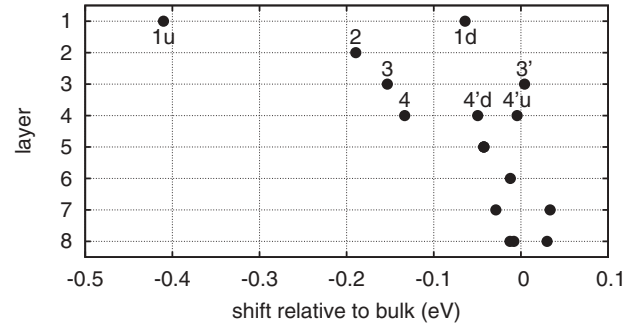


FIG. 4. Calculated Ge $3d$ core-level shifts at the Ge(001)- $c(4 \times 2)$ surface. The notation corresponds to that used in Fig. 3. The shifts are given with respect to the bulk line, which is obtained through an average of the Ge $3d$ core levels of the atoms belonging to the sixth, seventh, and eighth layers.

To minimize spurious interactions between the core hole and its images, the primitive cell is repeated four times for the calculation of Ge $3d$ core-level shifts. We thus use a tetragonal cell structure (cf. Fig. 3) with a lateral dimension of 30.7 bohr. The Brillouin zone is sampled with an off-centered $2 \times 2 \times 1$ \mathbf{k} -point mesh ensuring the same density of \mathbf{k} points as in the primitive surface cell calculations. For the adopted mesh, the smallest band gap is 0.35 eV. Figure 3 shows the different Ge sites of the reconstructed surface that we consider in our calculation of Ge $3d$ core-level shifts.

The calculated Ge $3d$ core-level shifts are shown in Fig. 4. The largest shifts with respect to the bulk line are found for the upper atoms of the buckled dimers (1u) which are less effective in charge screening because of electron depletion. The calculated values are compared to various experimental data in Table IX. Overall, the agreement between theory and experiment is very good with deviations of at most 0.1 eV. This level of agreement strengthens our theoretical approach and allows us to address with confidence more complex systems of which the structure has not yet fully been settled by experimental studies.

TABLE IX. Calculated Ge $3d$ core-level shifts at the Ge(001)- $c(4 \times 2)$ surface compared to available experimental data. The shifts are referred to the bulk line, which in the calculation is taken to correspond to average shift of the atoms belonging to the sixth, seventh, and eighth layers. All shifts are given in eV.

	Theory Present	Experiment			
		Ref. 50	Ref. 51	Ref. 52	Ref. 53
1u	-0.42	-0.51	-0.50	-0.43	-0.56
1d	-0.07	-0.10	–	–	–
2	-0.20	-0.23	-0.17	–	-0.24
3	-0.16	–	–	–	–
3'	0.00	–	–	–	–
4	-0.14	–	–	–	–
4'u	-0.01	–	–	–	–
4'd	-0.06	–	–	–	–

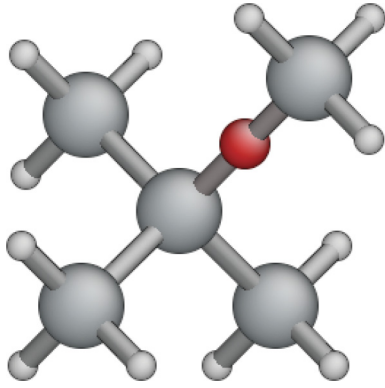


FIG. 5. (Color online) Ball and stick model of the idealized $\text{GeO}_1(\text{GeH}_3)_4$ molecule representing the oxidation state $n = 1$.

IV. CORE-LEVEL SHIFTS AT THE Ge/GeO₂ INTERFACE

A. Idealized Ge oxide molecules

To investigate the role of the local chemistry on the Ge $3d$ core-level shifts, we first study idealized Ge oxide molecules which reproduce the various oxidation states of Ge in the transition region. We consider $\text{GeO}_n(\text{GeH}_3)_4$ molecules, in which O atoms are inserted in n of the Ge-Ge bonds, with n varying between 0 and 4. For illustration, the $n = 1$ case is shown in Fig. 5. The Ge-O bond length and the Ge-O-Ge angle are kept fixed at 1.795 Å and 180°, respectively.

The calculated Ge $3d$ core-level shifts for such idealized molecules are given in Fig. 6. The shifts are calculated for varying oxidation state n and for varying fraction α of nonlocal exchange in the functional. The core-level shifts are found to be proportional to both oxidation state n and fraction α . At the PBE level, the core-level separation between the lowest ($n = 0$) and highest oxidation state ($n = 4$) is 2.0 eV. For $\alpha = 0.25$ and $\alpha = 1$, the separation increases to 2.25 eV and 3 eV, respectively.

B. Ge/GeO₂ interface models

Since the interface dipole contributes directly to the core-level shift across the interface, it is important to use a realistic description of the interfacial atomic structure. However, the bond pattern at the Ge/GeO₂ interface is at present essentially

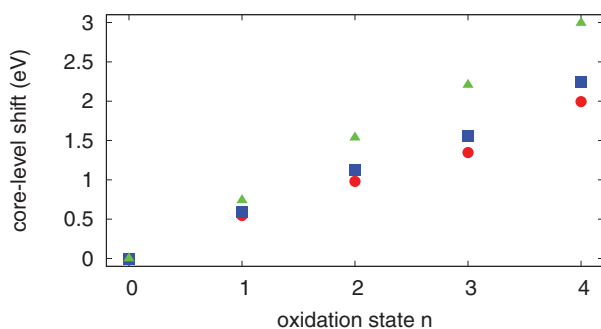


FIG. 6. (Color online) Calculated core-level shifts for the idealized $\text{GeO}_n(\text{GeH}_3)_4$ molecules vs oxidation state n . Circles (red), squares (blue), and triangles (green) correspond to calculations performed with PBE, PBE0, and PBEh($\alpha = 1.0$) functionals, respectively. The levels are referred to that of the oxidation state $n = 0$.

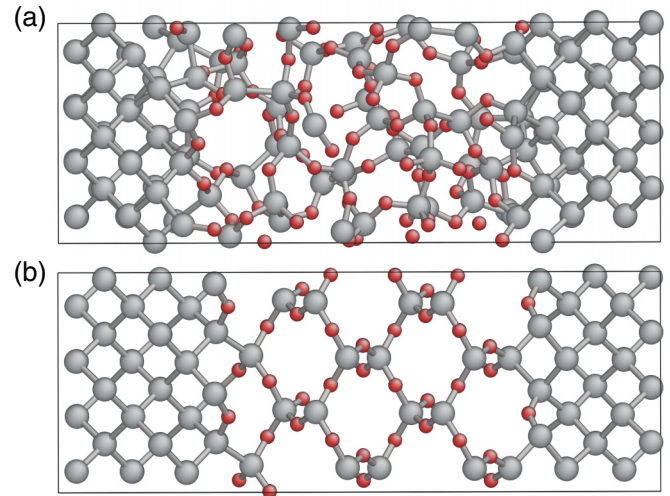


FIG. 7. (Color online) Atomic structure of two Ge/GeO₂ interface models used in this work, in which the oxide is either (a) amorphous or (b) crystalline. The balls representing the Ge atoms are light gray while those representing the O atoms are dark gray (red).

unknown. The two model structures which will be used in the present work are inspired from the structure at the Si/SiO₂ interface which has undergone extensive investigations.^{19,20,54} It should be understood that the present structures for the Ge/GeO₂ interface can only be validated through extensive comparisons with experimental data.

The first Ge/GeO₂ interface model comprises 217 atoms in a superlattice geometry with alternate layers of Ge and GeO₂ of approximately equal thickness [Fig. 7(a)]. In the interfacial plane, it has a $\sqrt{8} \times \sqrt{8}$ repeat unit with a side of 8.1 Å. The model was generated in Ref. 15 through full structural relaxations, which preserved the topology of its parent Si/SiO₂ interface structure.^{19,20,55} In short, the model shows a smooth transition region between crystalline Ge and amorphous GeO₂ with reasonable structural parameters and without any coordination defect, all Ge atoms being fourfold coordinated and all O atoms twofold coordinated. The transition region shows the appearance of all intermediate oxidation states of Ge (Ge⁺¹, Ge⁺², and Ge⁺³). The density of the GeO₂ region is 3.5 g/cm³. While the band gap of Ge vanishes in the PBE, the electronic structure at the interface does not show any metallic behavior, with a band gap evolving from 0.4 eV in the Ge layer to 2.6 eV in the GeO₂ layer. The finite gap in the Ge layer is mainly due to the quantum confinement effect.¹⁵ For a more detailed description of the structural and electronic properties of this model, we refer the reader to Refs. 15 and 16. In particular, this model has previously been used for the calculation of the valence band offset, resulting in a value of 3.4 eV.¹⁵

The second interface model also has superlattice geometry but the GeO₂ is found in a crystalline β -cristobalite phase [Fig. 7(b)]. The connection is achieved as in a similarly constructed model of the Si/SiO₂ interface and occurs without any coordination defect.^{37,56} In the interfacial plane, this model has the same repeat unit as the interface model with an amorphous oxide. The Ge layer consists of nine atomic layers of Ge (11.6 Å). Following a similar approach as for the first model,¹⁵ we allow the oxide to relax in the direction normal to the

interface, leading to a thickness of 21 Å and a density of 3.2 g/cm³. While this model is expected to show overall similar electronic properties as the first one, it carries the advantage of having a small interfacial repeat unit together with a C₈ rotational symmetry around an axis perpendicular to the interface. This allows one to achieve easy scaling of the model in the lateral directions. In particular, we also use models with interfacial repeat units containing 4, 16, and 32 interface Ge atoms.

C. Calculation of core-level shift through potential alignment

We are here interested in determining the Ge 3*d* core-level shift across the Ge/GeO₂ interface including the effect of the interface dipole. This corresponds to the shift ΔE_{XPS} between the oxidation state $n = 0$ in Ge and the oxidation state $n = 4$ in GeO₂. The interface also implies a dielectric discontinuity between the dielectric constants of Ge ($\epsilon = 16$) and GeO₂ ($\epsilon = 2.8$), which leads to difficulties in treating electrostatic screening effects in the core-hole calculations because of their long-range nature. Therefore, two different procedures will be applied to determine this shift. In the present section, we apply a method which is commonly used for the alignment of band structures at interfaces.^{57,58} All calculations in this section are performed with the pseudopotential-plane-wave scheme, first at the PBE level, and then with the PBE0 functional without further relaxing the atomic coordinates. The application of a more direct method is deferred to the next section.

The method we apply here consists of performing the core-hole calculations separately in bulk models of the two interface components. The interface model is only used to determine the line-up of a reference potential V_{ref} across the interface, which then allows us to connect the two bulk calculations. More specifically,

$$\Delta E_{\text{XPS}} = E_{\text{b}}^{\text{GeO}_2} - E_{\text{b}}^{\text{Ge}} + \Delta V_{\text{ref}} = \Delta E_{\text{b}} + \Delta V_{\text{ref}}, \quad (5)$$

where $E_{\text{b}}^{\text{GeO}_2}$ and E_{b}^{Ge} are obtained from bulk calculations in GeO₂ and Ge, respectively,

$$E_{\text{b}}^{\text{GeO}_2} = E_{+} + V_{\text{ref}}^{\text{GeO}_2} - E_0, \quad (6)$$

$$E_{\text{b}}^{\text{Ge}} = E_{+} + V_{\text{ref}}^{\text{Ge}} - E_0. \quad (7)$$

In particular, we note that in our pseudopotential scheme the calculations of both $E_{\text{b}}^{\text{GeO}_2}$ and E_{b}^{Ge} involve a same constant value, which is eliminated when taking the difference, $\Delta E_{\text{b}} = E_{\text{b}}^{\text{GeO}_2} - E_{\text{b}}^{\text{Ge}}$. The offset ΔV_{ref} of the reference potential across the interface,

$$\Delta V_{\text{ref}} = V_{\text{ref}}^{\text{Ge}} - V_{\text{ref}}^{\text{GeO}_2}, \quad (8)$$

is determined from the interface model calculation. We note that the calculations involving a positively charged core hole are in this way only performed for bulk models, where the total energy can be properly corrected.^{59,60} To deal with the long-range electrostatic effects in the bulk calculations, we applied a simple Madelung-like correction,^{59,60} as this correction has been demonstrated to be particularly accurate for well-localized charges.⁶¹ The calculation involving the interface model is only used for the potential alignment and is charge neutral. The fact that the electrostatic correction only needs to be applied to the bulk calculations is a clear advantage of the present potential-alignment method.

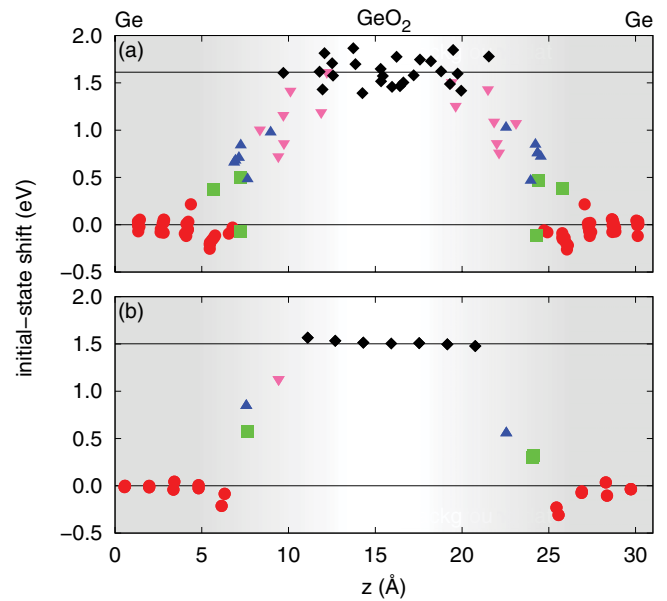


FIG. 8. (Color online) Initial-state Ge 3*d* core-level shifts across the Ge/GeO₂ interface as obtained within the PBE functional, for the model interface (a) with an amorphous oxide and (b) with a crystalline oxide, respectively. The various oxidation states are labeled: Ge⁰ (disks, red), Ge⁺¹ (squares, green), Ge⁺² (upwards-pointing triangles, blue), Ge⁺³ (downwards-pointing triangles, magenta), and Ge⁺⁴ (diamonds, black). The shifts are referred to the average shift of the central four Ge layers (lower horizontal line). The upper horizontal line corresponds to the average shift of the Ge⁺⁴ oxidation state in the central region of the oxide (13 Å < z < 19 Å).

As reference potential V_{ref} , we take the average electrostatic potential around the Ge nucleus. This is achieved through a Gaussian weight function with width of 0.175 bohr centered on the Ge atom. The variations of V_{ref} correspond to initial-state core-level shifts as obtained within a first-order perturbation scheme.³⁷ In this perspective, the term ΔE_{b} corresponds to the difference between the final-state core-hole relaxation energies in the two components.

We thus first address the initial-state shift by focusing on the potential offset ΔV_{ref} across the interface models. For both interfaces, we find that a $3 \times 3 \times 1$ **k**-point mesh yields fully converged initial-state shifts.⁶² The calculated initial-state shifts of the Ge core levels are shown in Fig. 8 for both our interface models. For the interface with an amorphous oxide, we find an initial-state shift of 1.6 eV when going from the center of the Ge layer to the center of the oxide layer. The interface with a crystalline oxide yields approximately the same value (1.5 eV). The initial-state shifts associated with intermediate oxidation states appear to be regularly spaced between the two limiting cases.

To accurately determine E_{b}^{Ge} in bulk Ge, we use cubic supercells of two different sizes (64 and 216 atoms). For each cell, the **k**-point sampling is increased symmetrically in all directions until the binding energies are found to be converged. For the 64-atom and 216-atom cells, we determine electrostatic corrections of 0.11 and 0.07 eV, respectively.⁶⁰ The scaling is fully consistent with the behavior of a point charge, thus allowing for straightforward extrapolation.

TABLE X. Core-level separation ΔE_{XPS} between Ge^0 and Ge^{+4} oxidation states across the Ge/GeO₂ interface, as obtained through the potential alignment method. We use two interface models which are distinguished by the nature of the oxide. The total core-level shift ΔE_{XPS} is the sum of the difference in initial-state shift (ΔV_{ref}) and in core-hole relaxation energy (ΔE_{b}) between the two interface components [cf. Eq. (5)]. The calculations are performed with PBE and PBE0 functionals. Energies are in eV.

Interface	Functional	ΔV_{ref}	ΔE_{b}	ΔE_{XPS}
Amorphous	PBE	1.60	0.94	2.54
β -cristobalite	PBE	1.50	1.13	2.63
Amorphous	PBE0	1.54	1.22	2.76
β -cristobalite	PBE0	1.52	1.23	2.75

Determining $E_{\text{b}}^{\text{GeO}_2}$ depends to some extent on the bulk model adopted for the oxide. We here consider two bulk GeO₂ structures which consistently reflect the respective structural arrangements in the two interface models. The first oxide structure corresponds to a model of amorphous GeO₂ generated previously via first-principles molecular dynamics.^{15,63} The structure contains 126 atoms at the experimental density (3.64 g/cm³) in a periodically repeated cubic unit cell and is composed of corner-sharing Ge(O_{1/2})₄ tetrahedra. The second oxide structure that we consider corresponds to the crystalline β -cristobalite phase. We ensure that our bulk model preserves the same structural arrangement found in the respective interface model. In this way, we construct two almost cubic supercells containing 48 and 384 atoms. The \mathbf{k} -point sampling in the Brillouin zone is increased until full convergence of the desired binding energies is achieved. However, it is found that Γ -point sampling is always sufficient, leading to errors of only 8 meV in the worst case, corresponding to the oxide with 48 atoms. For eliminating the spurious electrostatic interactions, we use Makov-Payne corrections.⁶⁰ For the amorphous model, this leads to an increase of the calculated binding energy by 0.58 eV. For the crystalline models of 48 and 384 atoms, the Makov-Payne corrections are 0.90 and 0.45 eV, respectively. The scaling is fully consistent with the point-charge behavior, thereby validating the use of these corrections.

In our pseudopotential approach, only the difference E_{b} between the binding energies in bulk Ge and bulk GeO₂ is physically meaningful and represents the difference in core-hole relaxation energy between the two interface components. The calculated values together with the initial-state shifts are given in Table X. The total core-level shift ΔE_{XPS} is obtained according to Eq. (5) and is found to be 2.5 eV for the interface with the amorphous oxide and 2.6 eV for the interface with the crystalline oxide. The two final values are thus very close, despite a slightly larger difference of about 0.2 eV found for the core-hole relaxation energies in the two bulk oxides.

To improve upon the PBE description, we also calculate the core-level separation ΔE_{XPS} with the hybrid PBE0 functional. The atomic structures obtained with the PBE functional are preserved without allowing for further relaxation, as this does not lead to any deterioration of the accuracy (cf. Sec. III B4). The calculation of the initial-state shifts in the interface models is performed with a \mathbf{k} -point sampling restricted to the sole Γ point, to further alleviate the numerical cost. On the

basis of PBE calculations with the same settings, this entails deviations of 0.1 eV with respect to full convergence for ΔV_{ref} . Assuming that the \mathbf{k} -point sampling errors do not depend on the functional, we use the PBE deviations to correct to PBE0 values of ΔV_{ref} . Table X shows that the initial-state shifts obtained in the PBE0 differ by less than 0.1 eV from those obtained in the PBE.

For the determination of the core-hole relaxation term ΔE_{b} , the \mathbf{k} -point sampling in the Ge bulk calculation is performed with the Baldereschi point,⁶⁴ while the Γ point is used for the bulk oxide models. On the basis of our PBE results, this reduced sampling does not give errors larger than 10 meV for ΔE_{b} . As shown in Table X, the calculated values of ΔE_{b} in the PBE0 are slightly larger than in the PBE. In conclusion of this section, we thus find that the potential alignment method yields, for both interface models, a full core-level shift ΔE_{XPS} of 2.75 eV at the PBE0 level of theory, up to 0.1–0.2 eV larger than found in the PBE.

D. Direct calculation of core-level shift followed by electrostatic correction

In this section, the Ge core-level shifts including the core-hole relaxation are directly determined through calculations involving the Ge/GeO₂ interface models. All calculations in this section are performed with the pseudopotential-plane-wave scheme, both at the PBE and PBE0 levels of theory. Since the interface models are in the superlattice geometry and subject to periodic boundary conditions, the dielectric environment affecting the core-hole relaxation is different than for an isolated interface. This difference is here accounted for within a classical electrostatics model and then used to correct the calculated values.

Core-level shifts are directly calculated for our two interface models. For both interfaces, we use a $3 \times 3 \times 1$ \mathbf{k} -point mesh. The calculated shifts are given in Fig. 9. In the PBE, the average separation ΔE_{XPS} between the core levels of Ge^0 and Ge^{+4} oxidation states is found to be ~ 2.0 eV for both interfaces (cf. Table XI). The shifts of the intermediate oxidation states lie in between, but the spacing between their average levels is no longer constant and increases with oxidation state, as the Ge screening becomes progressively less effective at increasing distance from the substrate.

Using the same atomic structures obtained in the PBE, we also perform core-level shift calculations at the PBE0 level for representative atoms chosen in the Ge and GeO₂ regions of the superlattice models (cf. Fig. 9). In these calculations, the Brillouin zone is sampled at the sole Γ point, but convergence corrections of the order of 0.08 eV are estimated from analogous calculations at the PBE level and incorporated in the final PBE0 result. As can be seen in Table XI, the values of ΔE_{XPS} obtained in the direct PBE0 calculations are larger than those obtained in the respective PBE calculations by 0.2–0.3 eV.

In these direct calculations, the total energy is obtained for a system with a positively charged core hole. The use of periodic boundary conditions requires the use of a uniform background charge to achieve charge neutrality in the simulation cell. Furthermore, the physical environment determined by the superlattice model significantly differs from the actual

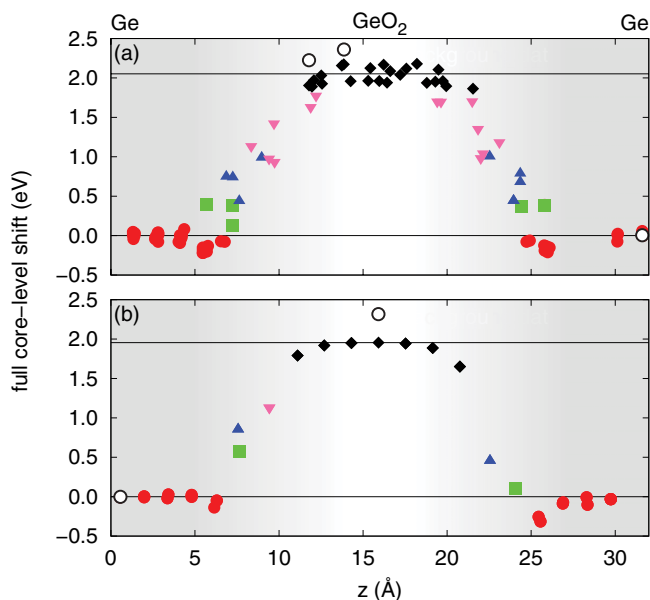


FIG. 9. (Color online) Full Ge 3d core-level shifts across the Ge/GeO₂ interface as obtained in the PBE, for the model interface (a) with an amorphous oxide and (b) with a crystalline oxide. Same notation as in Fig. 8. The three open circles correspond to calculations performed with the PBE0 functional.

environment due to a single interface. Hence, such calculations suffer from finite-size effects which are difficult to eliminate because of the long-range nature of the Coulomb potential. While several correction schemes have been proposed in the literature to deal with such effects in homogeneous dielectric media,^{60,65,66} similar schemes to treat dielectrically discontinuous systems have remained far less explored.

In the following, we develop such a correction scheme for interfaces in the superlattice geometry within a classical electrostatics model. In such a classical model, the interface components are distinguished by their dielectric constants and the core hole relaxation energy corresponds to the polarization energy of a positive unit charge. More specifically, we are interested in comparing the dielectric relaxation energy E_{per} of a core hole found in the middle of one of the superlattice

TABLE XI. Core-level separation ΔE_{XPS} between Ge⁰ and Ge⁺⁴ oxidation states across the Ge/GeO₂ interface, as obtained through direct calculation followed by classical electrostatics correction. We use two interface models which are distinguished by the nature of the oxide. The uncorrected results as obtained via direct calculations and the corrections pertaining to shifts on the Ge (δ_{Ge}) and GeO₂ (δ_{GeO_2}) sides of the interfaces are also provided. Calculations are performed with PBE and PBE0 functionals. Energies are in eV.

Interface	Functional	Corrections		ΔE_{XPS}	
		δ_{Ge}	δ_{GeO_2}	Direct	Corrected
Amorphous	PBE	0.03	0.33	2.05	2.41
β -cristobalite	PBE	0.01	0.36	2.00	2.37
Amorphous	PBE0	0.03	0.33	2.23	2.59
β -cristobalite	PBE0	0.01	0.36	2.30	2.66

layers with the respective energy E_{iso} of an isolated core hole in a bulk medium having the same dielectric constant as the layer. The desired correction is then given by $\delta = E_{\text{iso}} - E_{\text{per}}$. In our case, we need one such a correction for the Ge layer, δ_{Ge} , and one for the GeO₂ layer, δ_{GeO_2} .

For numerical convenience, the charge representing the core hole is modeled by a normalized Gaussian charge distribution centered at \mathbf{r}_0 ,

$$\rho(\mathbf{r}) = \frac{1}{\sqrt{2\pi}\sigma^2} e^{-(\mathbf{r}-\mathbf{r}_0)/(2\sigma^2)}, \quad (9)$$

where σ is the spread of the function and is taken to be equal to 1 bohr unless mentioned otherwise. The electrostatic energy of interest can be expressed as

$$U = \frac{1}{2} \int d^3r' \rho(\mathbf{r}') V(\mathbf{r}'), \quad (10)$$

where V is the electrostatic potential. This energy corresponds to the self-energy of the Gaussian charge distribution in the specified dielectric environment.

The determination of the electrostatics correction consists of determining the difference between the self-energy in a homogeneous dielectric medium and that in a periodic model representing the interface. In a homogeneous dielectric medium with a dielectric constant ϵ , the electrostatic self-energy U of the Gaussian charge distribution can be obtained analytically and corresponds to

$$E_{\text{iso}}(\epsilon) = \frac{1}{2\sigma\epsilon\sqrt{\pi}}. \quad (11)$$

In our classical electrostatics description, the superlattice model consists of alternating layers with dielectric constants of 16 for Ge and of 2.8 for GeO₂, as illustrated in Fig. 10(a). The local dielectric constant $\epsilon(z)$ varies smoothly for facilitating its numerical treatment, but the region of variation is taken to be much smaller than other distances involved. The size of the periodically repeated simulation cell and the thickness of the layers are set as in the density-functional calculation, unless mentioned otherwise. In this periodic simulation cell, the Gaussian charge distribution is compensated by a uniform background of opposite charge to avoid the divergence of the energy. The potential V appearing in Eq. (10) is obtained by addressing the Poisson equation for this system. We solve this equation numerically by describing the charge density and the potential on a three-dimensional mesh with a uniform spacing of 0.5 bohr.⁶⁷ The potential is then used in Eq. (10) to obtain U , which in this case corresponds to the electrostatic self-energy $E_{\text{per}}(z)$. We note that the self-energies defined by U in Eq. (10) depend on the spread σ and diverge for $\sigma \rightarrow 0$. On the opposite, the corrections $\delta = E_{\text{iso}} - E_{\text{per}}$ do not depend on σ insofar the distances to the interfaces are significantly larger than σ . This is numerically confirmed in Table XII.

Figure 10(b) shows the evolution of the electrostatic self-energy $U(z_0)$ as the center z_0 of the Gaussian charge distribution varies across the simulation cell. The corrections δ_{GeO_2} and δ_{Ge} are obtained by taking the difference between the self-energy calculated in the middle of the layers and the respective self-energies pertaining to the homogeneous bulk media, $E_{\text{iso}}(\epsilon_{\text{GeO}_2})$ and $E_{\text{iso}}(\epsilon_{\text{Ge}})$. We note that the correction is

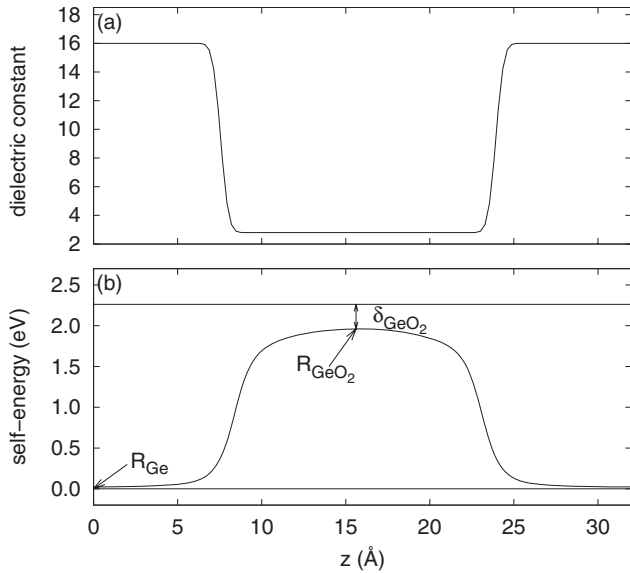


FIG. 10. (a) Local dielectric constant across the periodically repeated simulation cell varying nearly abruptly between the dielectric constant of Ge and that of GeO₂. (b) Electrostatic self-energy of a Gaussian charge distribution with $\sigma = 1$ bohr as its center varies across the periodically repeated simulation cell. The electrostatic energies E_{iso} corresponding to the same charge distribution in homogeneous dielectrics with dielectric constants of Ge and of GeO₂ are indicated by horizontal lines. The electrostatic corrections δ_{GeO_2} and δ_{Ge} are evaluated in the central positions R_{GeO_2} and R_{Ge} of the respective layers.

much larger in the GeO₂ than in the Ge layer, where the high dielectric constant effectively screens the inserted charge on a short distance.

We note that the correction defined in this way does not only correct the spurious electrostatic interactions due to the periodic boundary conditions but also eliminates the residual physical electrostatics effects due to the proximity of the interfaces in the periodic model. The latter feature satisfies our target of achieving by this correction the core-level shift between atoms situated on opposite sides of the interface but at large distances from the interface itself. Thus, the corrections defined in this way aim at achieving the same final result as that obtained through the potential alignment method applied in Sec. IV C.

To check the validity of the adopted corrections, we investigate how they perform for increasing lateral dimension L_x ($L_y = L_x$) of the periodic simulation cell. Focusing on the atomistic interface structure with crystalline oxide, we consider periodic models with square repeat units containing 4,

TABLE XII. Corrections δ_{Ge} and δ_{GeO_2} from classical electrostatics for various spreads σ of the Gaussian charge distribution. The corrections $\delta = E_{\text{iso}} - E_{\text{per}}$ are evaluated at the center of the respective layers in a simulation cell which corresponds to that used in the density functional calculations.

σ (bohr)	δ_{Ge} (eV)	δ_{GeO_2} (eV)
0.5	0.129	-0.106
1.0	0.130	-0.103
1.5	0.131	-0.097

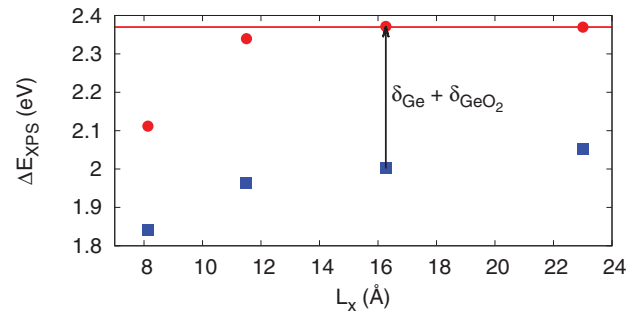


FIG. 11. (Color online) Ge 3d core-level shifts (squares, blue) calculated within the PBE functional for a series of periodic Ge/GeO₂ interface models with crystalline oxides showing different lateral dimensions L_x ($L_y = L_x$). The periodicity and the layer thicknesses in the vertical direction are kept fixed and correspond to the model introduced in Sec. IV B. The core-level shift is taken between atoms at the centers of the Ge and GeO₂ layers. Core-level shifts including δ_{GeO_2} and δ_{Ge} corrections from classical electrostatics (cf. Fig. 10) are also shown (disks, red). The horizontal line corresponds to the converged result inferred from the calculations.

8, 16, and 32 interfacial Ge atoms, which correspond to lateral dimensions L_x of 8.2, 11.6, 16.4, and 23.2 Å, respectively. The size of the supercell in the vertical direction is kept fixed. For these models, we calculate the total energies for Ge 3d core holes located in the middle of the Ge and GeO₂ layers and derive the corresponding shift ΔE_{XPS} between Ge⁰ and Ge⁺⁴ oxidation states. The calculated values are reported in Fig. 11 as a function of the lateral side of the supercell. The calculated core-level shift is found to increase monotonically with lateral side. Then, we calculate within classical electrostatics, the corrections δ_{GeO_2} and δ_{Ge} for periodic superlattice models with the same supercell as the atomistic models. When the corrections from classical electrostatics are added to the calculated shifts, one clearly observes that the shifts reach convergence. In particular, at $L_x = 11.6$ Å, corresponding to the side used for the Ge/GeO₂ interface models in Sec. IV B, the deviation from the converged result is lower than 0.03 eV. The larger deviations at $L_x = 8.2$ Å indicate that the correction from classical electrostatics is insufficient and suggest that quantum-mechanical effects due to the relatively close periodic images might still be operative.⁶⁸

From the present analysis, we infer that the model interfaces with a lateral side of $L_x = 11.6$ Å give sufficiently accurate results provided the corrections of classical electrostatics are included. These corrections apply indifferently to core-level shifts calculated in the PBE and in the PBE0. The corrected values of the ΔE_{XPS} shifts for the two model interfaces considered are reported in Table XI. The two interface models give consistent values, around 2.4 in the PBE and around 2.6–2.7 eV in the PBE0.

V. DISCUSSION AND CONCLUSION

Table XIII summarizes the main result of this work which corresponds to the theoretical determination of the Ge 3d core-level shift ΔE_{XPS} between Ge⁰ and Ge⁺⁴ oxidation states at the Ge/GeO₂ interface. This shift is calculated through two different methods and for two different interface models. We

TABLE XIII. Comparison between calculated core-level shift ΔE_{XPS} for the two interface models considered in this work as obtained through the potential alignment method (Sec. IV C) and through direct calculation with addition of electrostatic corrections (Sec. IV D). The calculations refer to PBE and PBE0 functionals. Energies are in eV.

Interface	Functional	Potential alignment	Direct with corrections
Amorphous	PBE	2.54	2.41
β -cristobalite	PBE	2.63	2.37
Amorphous	PBE0	2.76	2.59
β -cristobalite	PBE0	2.75	2.66

find an rms deviation of 0.18 eV between the two different methods. Since the two applied methods target the same physical quantity ΔE_{XPS} , this residual deviation solely reflects the numerical difficulty in achieving a converged result for a given interface model.

The difference between the two interface structures is always smaller than 0.1 eV, despite the different interfacial bond pattern in the two models. Nevertheless, the two models also have features in common. Indeed, both interface structures show no coordination defects and a similar bond density reduction, thus reproducing the main features of their parent Si/SiO₂ interface models. Hence, the close agreement for ΔE_{XPS} further confirms that the interface dipole does not differ significantly among models satisfying such conditions, as previously found in investigations of band offsets.^{18,69}

Considering on the same footing the results obtained for different models and through different methods, we find $\Delta E_{\text{XPS}} = 2.49$ eV in the PBE and $\Delta E_{\text{XPS}} = 2.69$ eV in the PBE0, with respective rms deviations of 0.10 and 0.07 eV. In the following, the discussion is based on the result obtained in the PBE0, which is expected to yield a closer agreement with experiment (cf. Sec. III).

Experimental determinations of ΔE_{XPS} are found to depend on the growth procedure used for the Ge/GeO₂ interface. Interfaces with oxides grown by thermal oxidation in O₂ atmosphere generally give $\Delta E_{\text{XPS}} \cong 3.3$ eV,^{3–8} but much larger values (3.7–3.8 eV) are found in experiments in which the oxidation is achieved with O₃ and atomic O.^{9,10} Our PBE0 value of 2.7 eV is significantly lower than all available experimental determinations. The discrepancy is much larger than both the numerical error with which we determine ΔE_{XPS} and the expected accuracy associated with the PBE0 level of theory. This leads to the conclusion that the Ge/GeO₂ interface structure differs from those represented by the adopted model structures. In other terms, the interface structure that appears to give a satisfactory description of the Si/SiO₂ interface^{19,35} does not provide an acceptable description of the *a priori* analogous Ge/GeO₂ interface.

This conclusion, which follows from the comparison between theoretical and experimental ΔE_{XPS} , reinforces an analogous conclusion reached on the basis of a comparison between calculated and measured valence band offsets.¹⁵ Indeed, a previous theoretical investigation determined a valence band offset of 3.4 eV for one of the model interface structures studied in the present work.¹⁵ This value is significantly lower

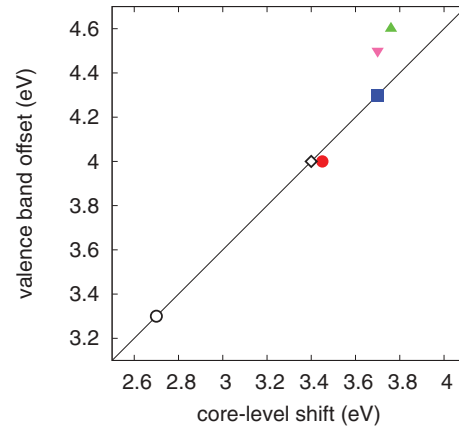


FIG. 12. (Color online) Ge 3d core-level shift ΔE_{XPS} and valence band offset (VBO) as determined theoretically (open symbols) and experimentally (solid symbols) for a given Ge/GeO₂ interface model or sample. The circle corresponds to the model interface with an amorphous oxide (ΔE_{XPS} from the present work and VBO from Ref. 15). The straight line is consistent with our calculated values but allows for an undetermined contribution to the interface dipole, for example, as resulting from the valence alternation pair in Ref. 18 (diamond). The VBOs corresponding to the red disk (Ref. 5) and the blue square (Ref. 9) are obtained through valence-band photoemission, while those corresponding to the magenta downward-pointing (Ref. 9) and green upward-pointing triangles (Ref. 10) are derived through Kraut's method.

than found in experimental studies which yield values ranging between 4.0 and 4.5 eV.^{5,9,10}

In Fig. 12, calculated and measured values are compared in a VBO- ΔE_{XPS} plot. Only experimental data corresponding to ΔE_{XPS} and VBO determined for the same sample are considered. The experimental VBOs are either determined through valence-band photoemission or through the use of Kraut's method. The spread of the available experimental data clearly indicates that the interface dipole depends on the sample at hand. However, an uncontrolled contribution to the interface dipole affects the core-level shift and the valence band offset by the same amount. It is therefore meaningful to compare the calculated results with experiment allowing for an undetermined contribution to the interface dipole. This results in the straight line in Fig. 12. Overall, the available experimental results are consistent with the intrinsic relation between ΔE_{XPS} and VBO found in the calculation. In particular, the data corresponding to VBOs measured through valence-band photoemission show excellent agreement, while the VBOs obtained with Kraut's method are only slightly larger. This result strengthens the results of our calculations and suggests that the difference between the theoretical and the various experimental interface structures only lies in their interface dipole.

The actual interface structure at Ge/GeO₂ interfaces remains an open question. There have been several investigations indicating that substoichiometric germanium oxide is intrinsically different than its silicon counterpart.^{17,22,70–72} In particular, Binder *et al.* performed first-principles molecular dynamics on substoichiometric GeO_x finding a structure with a high concentration of negatively charged threefold coordinated

Ge atoms and positively charged threefold coordinated O atoms.²² Bonding motifs of this kind carrying opposite charge are known as valence alternation pairs.⁷³ It has been shown that when these pairs are properly oriented with respect to the interface a sizable contribution to the interface dipole can be obtained.¹⁸ This offers a possible interpretation scheme which could reconcile the theoretical and experimental values for ΔE_{XPS} and the VBO. However, also other mechanisms might affect the interface dipole, such as the charge trapping in point defects or the occurrence of high or low density layers in the transition region. It should be noted that the interface dipole required to move in the direction of the experimental data should oppose the natural dipole created by the electronegativity difference in the Ge-O bond.¹⁸

In summary, this work focuses on the Ge $3d$ core-level shift at Ge/GeO₂ interfaces. It is first demonstrated that such core-level shifts are reliably described within semilocal and hybrid density functional schemes through comparison with experiment for a set of Ge-based molecules. Then, the numerical problem consisting in determining such shifts for interface models subject to periodic boundary conditions is addressed. Two different strategies are pursued and found to yield consistent results. The most reliable theoretical estimate of the Ge $3d$ core-level shift is found to be significantly lower than found in experimental studies. However, the theoretical

core-level shift is found to deviate from measured shifts in the same way as the calculated valence band offset does from respective experimental data. This result suggests that the theoretical relation between core-level shift and valence band offset is consistent with experimental data. The deviation from experiment resides in the actual interface dipole at the interface, which is apparently not well reproduced in the structural models of the Ge/GeO₂ interface used so far. Since these models are inspired from the structure at the Si/SiO₂ interface, we reach the conclusion that the atomic structure at Ge/GeO₂ interfaces must be inherently different. Identifying the bonding pattern at this interface appears as a priority issue in view of envisaging valid strategies for defect passivation.

ACKNOWLEDGMENTS

We thank G. Pourtois for providing us with the pseudopotentials used in Ref. 14, C. Corminboeuf for financing the ADF software license at EPFL, A. Molle and M. Perego for sharing with us their analysis of measured core-level shifts, and O. V. Yazyev for help in the use of the ADF code. Financial support from the Swiss National Science Foundation (Grants No. 200020-119733/1, No. 206021-128743, and No. 200020-134600/1) is acknowledged. We used computational resources of CSCS and CSEA.

*Present address: Department of Chemistry, Uppsala University, Uppsala, Sweden.

¹M. Houssa, A. Satta, E. Simoen, B. D. Jaeger, M. Meuris, M. Caymax, and M. Heyns, in *Germanium-Based Technologies* (Elsevier, Oxford, 2007), pp. 233–265.

²V. V. Afanas'ev, A. Stesmans, A. Delabie, F. Bellenger, M. Houssa, and M. Meuris, *Appl. Phys. Lett.* **92**, 022109 (2008).

³D. Schmeisser, R. Schnell, A. Bogen, F. Himpsel, D. Rieger, G. Landgren, and J. Morar, *Surf. Sci.* **172**, 455 (1986).

⁴K. Prabhakaran and T. Ogino, *Surf. Sci.* **325**, 263 (1995).

⁵A. Ohta, H. Nakagawa, H. Murakami, S. Higashi, and S. Miyazaki, *e-J. Surf. Sci. and Nanotech.* **4**, 174 (2006).

⁶M. Caymax, S. V. Elshocht, M. Houssa, A. Delabie, T. Conard, M. Meuris, M. Heyns, A. Dimoulas, S. Spiga, M. Fanciulli, J. Seo, and L. Goncharova, *Mater. Sci. Eng. B* **135**, 256 (2006).

⁷A. Molle, M. N. K. Bhuiyan, G. Tallarida, and M. Fanciulli, *Appl. Phys. Lett.* **89**, 083504 (2006).

⁸K. Kita, S. Wang, M. Yoshida, C. Lee, K. Nagashio, T. Nishimura, and A. Toriumi, in *Electron Devices Meeting (IEDM), 2009 IEEE International* (2009), pp. 1–4.

⁹M. Perego, G. Scarel, M. Fanciulli, I. L. Fedushkin, and A. A. Skatova, *Appl. Phys. Lett.* **90**, 162115 (2007).

¹⁰M. Yang, R. Q. Wu, Q. Chen, W. S. Deng, Y. P. Feng, J. W. Chai, J. S. Pan, and S. J. Wang, *Appl. Phys. Lett.* **94**, 142903 (2009).

¹¹E. A. Kraut, R. W. Grant, J. R. Waldrop, and S. P. Kowalczyk, *Phys. Rev. Lett.* **44**, 1620 (1980).

¹²S. A. Chambers, T. Droubay, T. C. Kaspar, and M. Gutowski, *J. Vac. Sci. Technol. B* **22**, 2205 (2004).

¹³M. Houssa, G. Pourtois, M. Caymax, M. Meuris, and M. Heyns, *Surf. Sci.* **602**, L25 (2008).

¹⁴G. Pourtois, M. Houssa, A. Delabie, T. Conard, M. Caymax, M. Meuris, and M. M. Heyns, *Appl. Phys. Lett.* **92**, 032105 (2008).

¹⁵P. Broqvist, J. F. Binder, and A. Pasquarello, *Appl. Phys. Lett.* **94**, 141911 (2009); **98**, 129901 (2011).

¹⁶P. Broqvist, J. F. Binder, and A. Pasquarello, *Microelectron. Eng.* **86**, 1589 (2009).

¹⁷L. Lin, K. Xiong, and J. Robertson, *Appl. Phys. Lett.* **97**, 242902 (2010).

¹⁸P. Broqvist, J. F. Binder, and A. Pasquarello, *Microelectron. Eng.* **88**, 1467 (2011).

¹⁹A. Bongiorno, A. Pasquarello, M. S. Hybertsen, and L. C. Feldman, *Phys. Rev. Lett.* **90**, 186101 (2003).

²⁰A. Bongiorno and A. Pasquarello, *Appl. Phys. Lett.* **83**, 1417 (2003).

²¹A. Alkauskas, P. Broqvist, F. Devynck, and A. Pasquarello, *Phys. Rev. Lett.* **101**, 106802 (2008).

²²J. F. Binder, P. Broqvist, and A. Pasquarello, *Appl. Phys. Lett.* **97**, 092903 (2010).

²³J. P. Perdew, K. Burke, and M. Ernzerhof, *Phys. Rev. Lett.* **77**, 3865 (1996).

²⁴J. P. Perdew, M. Ernzerhof, and K. Burke, *J. Chem. Phys.* **105**, 9982 (1996).

²⁵D. D. Koelling and B. N. Harmon, *J. Phys. C* **10**, 3107 (1977).

²⁶A. Dal Corso, A. Pasquarello, A. Baldereschi, and R. Car, *Phys. Rev. B* **53**, 1180 (1996).

²⁷P. Giannozzi, S. Baroni, N. Bonini, M. Calandra, R. Car, C. Cavazzoni, D. Ceresoli, G. L. Chiarotti, M. Cococcioni, I. Dabo, A. Dal Corso, S. de Gironcoli, S. Fabris, G. Fratesi, R. Gebauer, U. Gerstmann, C. Gougoussis, A. Kokalj, M. Lazzeri, L. Martin-Samos, N. Marzari, F. Mauri, R. Mazzarello, S. Paolini, A. Pasquarello, L. Paulatto, C. Sbraccia, S. Scandolo, G. Sclauzero, A. P. Seitsonen, A. Smogunov, P. Umari, and R. M. Wentzcovitch, *J. Phys.: Condens. Matter* **21**, 395502 (2009).

²⁸G. te Velde, F. M. Bickelhaupt, E. J. Baerends, C. Fonseca Guerra, S. J. A. van Gisbergen, J. G. Snijders, and T. Ziegler, *J. Comput. Chem.* **22**, 931 (2001).

- ²⁹E. van Lenthe, E. J. Baerends, and J. G. Snijders, *J. Chem. Phys.* **99**, 4597 (1993).
- ³⁰N. Troullier and J. L. Martins, *Phys. Rev. B* **43**, 1993 (1991).
- ³¹P. Broqvist, A. Alkauskas, and A. Pasquarello, *Phys. Rev. B* **80**, 085114 (2009).
- ³²H.-V. Nguyen and S. de Gironcoli, *Phys. Rev. B* **79**, 205114 (2009).
- ³³W. F. Egelhoff, *Surf. Sci. Rep.* **6**, 253 (1987).
- ³⁴E. Pehlke and M. Scheffler, *Phys. Rev. Lett.* **71**, 2338 (1993).
- ³⁵O. Yazyev and A. Pasquarello, *Phys. Rev. Lett.* **96**, 157601 (2006).
- ³⁶A. Pasquarello, M. S. Hybertsen, and R. Car, *Phys. Rev. Lett.* **74**, 1024 (1995).
- ³⁷A. Pasquarello, M. S. Hybertsen, and R. Car, *Phys. Rev. B* **53**, 10942 (1996).
- ³⁸A. Pasquarello, M. Hybertsen, and R. Car, *Phys. Scr.* **T66**, 118 (1996).
- ³⁹A. Alkauskas, P. Broqvist, and A. Pasquarello, *Phys. Rev. Lett.* **101**, 046405 (2008).
- ⁴⁰A. Alkauskas, P. Broqvist, and A. Pasquarello, *Phys. Status Solidi B* **248**, 775 (2011).
- ⁴¹P. Broqvist, A. Alkauskas, and A. Pasquarello, *Phys. Rev. B* **78**, 075203 (2008).
- ⁴²A. A. Bakke, H.-W. Chen, and W. L. Jolly, *J. Electron Spectrosc. Relat. Phenom.* **20**, 333 (1980).
- ⁴³J. L. Hencher and F. J. Mustoe, *Can. J. Chem.* **53**, 3542 (1975).
- ⁴⁴K. Ohno, H. Matsuura, Y. Endo, and E. Hirota, *J. Mol. Spectrosc.* **118**, 1 (1986).
- ⁴⁵A. D. Caunt, H. Mackle, and L. E. Sutton, *Trans. Faraday Soc.* **47**, 943 (1951).
- ⁴⁶L. A. Curtiss, P. C. Redfern, K. Raghavachari, and J. A. Pople, *J. Chem. Phys.* **109**, 42 (1998).
- ⁴⁷A. Alkauskas and A. Pasquarello, *Phys. Rev. B* **84**, 125206 (2011).
- ⁴⁸T. Deegan and G. Hughes, *Appl. Surf. Sci.* **123-124**, 66 (1998).
- ⁴⁹We submitted the pseudopotentials used in Ref. 14 to a similar comparison against all-electron results focusing on the core-level shift between the idealized Ge(GeH₃)₄ and Ge(OGeH₃)₄ molecules (cf. Sec. IV A). This test revealed an enhanced shift by 0.59 eV with respect to the corresponding all-electron shift, to be compared with the deviation of 0.05 eV found within the present pseudopotential scheme.
- ⁵⁰P. E. J. Eriksson and R. I. G. Uhrberg, *Phys. Rev. B* **81**, 125443 (2010).
- ⁵¹E. Landemark, C. J. Karlsson, L. S. O. Johansson, and R. I. G. Uhrberg, *Phys. Rev. B* **49**, 16523 (1994).
- ⁵²R. D. Schnell, F. J. Himpsel, A. Bogen, D. Rieger, and W. Steinmann, *Phys. Rev. B* **32**, 8052 (1985).
- ⁵³G. Le Lay, J. Kanski, P. O. Nilsson, U. O. Karlsson, and K. Hricovini, *Phys. Rev. B* **45**, 6692 (1992).
- ⁵⁴A. Pasquarello, M. S. Hybertsen, and R. Car, *Nature (London)* **396**, 58 (1998).
- ⁵⁵F. Giustino and A. Pasquarello, *Phys. Rev. Lett.* **95**, 187402 (2005).
- ⁵⁶A. Pasquarello, M. S. Hybertsen, and R. Car, *Appl. Surf. Sci.* **104-105**, 317 (1996).
- ⁵⁷C. G. Van de Walle and R. M. Martin, *Phys. Rev. B* **34**, 5621 (1986).
- ⁵⁸A. Baldereschi, S. Baroni, and R. Resta, *Phys. Rev. Lett.* **61**, 734 (1988).
- ⁵⁹M. Leslie and N. J. Gillan, *J. Phys. C* **18**, 973 (1985).
- ⁶⁰G. Makov and M. C. Payne, *Phys. Rev. B* **51**, 4014 (1995).
- ⁶¹H.-P. Komsa, T. Rantala, and A. Pasquarello, *Physica B* **407**, 3063 (2012).
- ⁶²A denser mesh yielded changes of initial core-level shifts lower than 5 meV. A single **k** point was used in the *z* direction because of the slab geometry. This results in an isotropically uniform **k**-point density.
- ⁶³J. F. Binder, P. Broqvist, and A. Pasquarello, *Microelectron. Eng.* **88**, 391 (2011).
- ⁶⁴A. Baldereschi, *Phys. Rev. B* **7**, 5212 (1973).
- ⁶⁵S. Lany and A. Zunger, *Phys. Rev. B* **78**, 235104 (2008).
- ⁶⁶C. Freysoldt, J. Neugebauer, and C. G. Van de Walle, *Phys. Rev. Lett.* **102**, 016402 (2009).
- ⁶⁷J. D. Jackson, *Classical Electrodynamics*, 3rd ed. (Wiley, New York, 1998); H.-P. Komsa and A. Pasquarello (unpublished).
- ⁶⁸S. E. Taylor and F. Bruneval, *Phys. Rev. B* **84**, 075155 (2011).
- ⁶⁹F. Giustino, A. Bongiorno, and A. Pasquarello, *J. Phys.: Condens. Matter* **17**, S2065 (2005).
- ⁷⁰J. F. Binder, P. Broqvist, and A. Pasquarello, *Microelectron. Eng.* **86**, 1760 (2009).
- ⁷¹L. Tsetseris and S. T. Pantelides, *Appl. Phys. Lett.* **95**, 262107 (2009).
- ⁷²J. F. Binder, P. Broqvist, and A. Pasquarello, *Physica B* **407**, 2939 (2012).
- ⁷³M. Kastner, D. Adler, and H. Fritzsche, *Phys. Rev. Lett.* **37**, 1504 (1976).